Model of platelet transport in flowing blood with drift and diffusion terms

Eugene C. Eckstein and Fethi Belgacem
Department of Biomedical Engineering, University of Miami, Coral Gables, Florida 33124 USA

ABSTRACT A drift term is added to the convective diffusion equation for platelet transport so that situations with near-wall excesses of platelets can be described. The mathematical relationship between the drift and the fully developed, steady-state platelet concentration profile is shown and a functional form of the drift that leads to concentration profiles similar to experimentally determined profiles is provided. The transport equation is numerically integrated to determine concentration profiles in the developing region of a tube flow. With the approximate drift function and typical values of augmented diffusion constant, the calculated concentration profiles have near-wall excesses that mimic experimental results, thus implying the extended equation is a valid description of rheological events. Stochastic differential equations that are equivalent to the convective diffusion transport equation are shown, and simulations with them are used to illustrate the impact of the drift term on platelet concentration profiles during deposition in a tube flow.

INTRODUCTION

Researchers have shown that platelet concentration profiles in flowing blood have excess concentrations near the walls (1–16). Because calculations with the existing equations for platelet transport do not predict these excesses, there is good reason to examine the models of platelet transport and extend the platelet transport equation. The extended equation shown in this paper assumes that platelet motions can be separated into random and deterministic portions. Furthermore, it assumes that the deterministic portion of the lateral motion can be described by a drift function with a shape that is determined from the fully developed, steady-state concentration profile for platelets. The deterministic portion describes those flow-associated events that act to redistribute the platelets to particular locations. Convective motion in the axial direction is a familiar example of a deterministic motion. The inclusion of a position-dependent, directed lateral motion in the extended equation leads to concentration profiles with excesses. Diffusive motions are described by the random portion, and as usual for blood flows, their description entails use of an augmented diffusion coefficient. Like most prior treatments of platelet tansport, the extended equation is a single component description; it implicitly includes effects due to red cells and plasma by the use of an augmented diffusion constant and the drift function. The drift team is introduced to describe rheological events that are not encompassed by the use of an augmented diffusion coefficient.

An extended relationship for platelet transport is an important step toward developing a quantitative description of thrombosis. Because flow often establishes near-wall excesses of platelets, it affects the availability of these key participants in the thrombotic process. Such events are usually classified in qualitative descriptions of thrombosis as rheological aspects. With a transport relationship that fully describes the rheological aspects of platelet transport, a complete quantitative description of the thrombotic process should be possible. Producing such a model will be a significant challenge because the model must include delivery, reactions, interactions, and removal of platelets and many other species.

The material below is arranged in a way that provides a physical rationale for the extended transport equation and illustrates its features. Prior work is reviewed in the next section to show the character of near-wall excesses and the rheological conditions associated with them. The experimental studies, concepts, and analogies underlying the original description of flow-enhanced platelet transport relationship are examined. Experiments showing directed (nonrandom) lateral motions of particles are briefly reviewed. The key parts of the middle section describe the concept of platelet transport with a flow-induced drift, the relationship of the drift to the fully developed, steady-state concentration profile, the deriva tion of an extended convective diffusion equation, and

Address correspondence to Eugene C. Eckstein, Department of Biomedical Engineering, University of Miami, P.O. Box 248294, Coral Gables, FL 33124.

0006-3495/91/07/53/17 $2.00

the relationship with its equivalent set of stochastic differential equations. The following section contains a description of the methods for numerical analysis and computational studies of these equations. Sequences of concentration profiles for the axial development of the near-wall excess are shown as computed by both the extended convective diffusion equation and the stochastic differential equations. Also, sequences of concentration profiles in the axial direction and amounts of deposition at various axial stations are shown for cases where platelets can adhere to the wall. These sequences show that the extended transport equations predict that a near-wall excess occurs even when the bounding surface is highly reactive.

RELATED PRIOR WORK

Observations of nonuniform concentration profiles in nonreactive situations[1]

Several groups have observed concentration profiles with near-wall excesses of platelets (in vivo [1], in vitro [2–4]) or of platelet-sized latex beads (5–9). Also, investigations have shown indirect evidence of near-wall excesses of platelets, including effects associated with skimming of higher near-wall concentrations during flow from larger to smaller tubes in T junctions (10–16). It has been demonstrated that red blood cells (RBC) are necessary for flow-induced, near-wall excesses (2–5, 7, 8). Large excesses consistently occur for certain combinations of bead size (2 μm or more), suspension hematocrit (15–50%), and shear rate (those flows where the stress in the near-wall region is sufficient to deform the RBC) (6, 9). Near-wall excesses have been observed in vessels of 25 μm diameter (1), in tubes of 3 mm diameter (2), and, in our work, in channels and tubes of intermediate height and diameter (5–9). In vitro studies with suspensions of RBC and latex beads have shown that the concentration profile has a peak that is slightly off the wall (from 3–6 μm) and that the axial development of the profile in 200-μm tubes appears to be completed in the first 2 cm (8).

Shear-enhanced lateral motions in tube flows of suspensions

The traditional convective diffusion equation used to model platelet transport in flowing blood is built upon the assumption that the relevant events can be described in terms of a dilute, single component, the platelets, in a "solvent" (17). The solvent represents both the red cells and plasma; no accommodation is made for the different percentages of red cells and plasma that occupy various lateral locations in a channel or tube flow. Augmented diffusion coefficients are used because the lateral motions of platelets in sheared RBC suspensions are known to be much larger than the Brownian motions in an equivalent stationary system. Goldsmith used a traveling microtube apparatus to track the motions of platelet-sized latex beads in low shear-rate blood flows; with measurements of the change of lateral position over a fixed time interval and the formula for the diffusive motion of an unbiased random walk, he computed a coefficient for augmented diffusion (18). Turitto et al. used Taylor's method to measure the effective lateral diffusion coefficient in blood flow through a 200-μm tube (14). In a review of hemodynamic concepts, Goldsmith and Turitto note that their measurements of the augmented diffusivity are in fair agreement (19). An important point is that Turitto et al. could use Taylor's method only when the shear rate was low, because, as noted in an appendix to their paper, nonuniform distributions of platelets occurred in flows with wall shear rates of 440 inverse seconds and higher (14). Values for platelet diffusivity at high wall shear rates have been deduced by applying transport theory models to measurements of platelet deposition on surfaces (20). Shear augmented diffusion is also a factor in oxygen transport (21) and hemofiltration (22); augmented diffusion coefficients are commonly used in descriptions of these processes.

Analogies

Our understanding of flow-enhanced lateral platelet motions is aided by two analogies. An analogy with the kinetic theory of gases considers that the shear flow causes the platelets to have collisions[2] with the other suspended cells. Because of these collisions each platelet has random lateral movements that are described by random walk theory. The collisions and the changing casts of nearest neighbors occur because particles at

[1]This section focuses on nonuniform profiles in nonreactive situations because cases involving reaction and deposition are expected to have concentration gradients associated with delivery of materials to the reactive site.

[2]The convenient term collision prompts two comments. First, collisions cause motions in both the axial and lateral directions; however, the extra axial motion is often disregarded bacause it is small compared to the axial motion associated with conventional convection. Second, the term collision is convenient, but inaccurate; a truer depiction is that of strong interactions among the particles. In a dilute suspension, the interactions are sporadic and isolated because the particles are far apart. In a concentrated suspension, there is no obvious or convenient beginning or end of an interaction; each particle is always strongly interacting with its many neighbors.

different lateral locations in a shear flow have different velocities. This picture has its roots in the microrheological studies of S. G. Mason and coworkers, (for a review, see reference 23) particularly in their studies of dilute suspensions. They showed that no lateral motion resulted from the collision of a pair of rigid spheres in a low Reynolds number shear flow. Lateral motion did occur when the Reynolds number was increased or when flexible particles were used. The mathematical basis for the analogy invokes a central limit theorem to predict the net outcome of many small changes of lateral position, the Gaussian distribution, which is also a result of a simple random walk.

The second analogy, proposed by Keller (24), focuses on the fluid around the suspended particles. The shearing flow of the suspension causes each particle to have a rotary motion that acts to "stir" the suspending fluid near it; each particle and its nearby fluid is likened to a turbulent eddy. This stirring motion mixes the adjacent material with that on nearby streamlines. The analogy is intuitively attractive for situations involving small molecules that are dissolved in the suspending fluid, but it also extends to particles that are of roughly the same size as the suspended stirring particles. The outcome of the stirring is characterized as an enhancement of the diffusive motion that would accompany a concentration gradient caused by external events.

Consideration of the above analogies shows that the use of an augmented diffusion coefficient in the existing platelet transport equation is, while reasonable, *ad hoc.* Values of the augmented diffusion coefficient are obtained by fitting experimental data to solutions of the differential equations for the particular experimental geometry. The lateral drift of the platelet transport model below is introduced in the same spirit.

Nonrandom lateral motions

Because the lateral drift that is used below has a fixed direction at each point, it is useful to note other situations where particles are known to move laterally in directed, nonrandom ways. Flexible particles in dilute suspensions are known to drift toward the centerline regardless of the Reynolds number (23). For flows with an inertial component, rigid particles will move to particular lateral positions; the best known example is the Segré-Silberberg effect, which requires a very small inertial component (25). In concentrated suspensions, there is a near-wall region, usually termed a marginal layer, that is deficient in particles as compared with the central region (26, 27). In blood flow this layer's dimension is usually attributed to a combination of geometric interference and inward migration of the flexible erythrocytes.

RHEOLOGICAL POTENTIAL

The novel feature of this model is the explicit inclusion of a drift team, a directed motion that is set equal to the negative gradient of a potential. Use of a drift term was prompted by inspection of the mathematical descriptions of other mechanical systems that include both directed and random motions, e.g., the kinetic theory of gases. There, the terms convective and diffusive are used respectively in place of directed and random. The theory of stochastic processes provides methods to determine and characterize the random motions, and in a sense, provides the basis for describing "shear-augmented" diffusion. That theory contains a classical problem and solution that are useful for depicting directed motions of platelets in flowing blood (28). The problem involves the motion of a particle in a potential field. In this problem, the particle is at all times subject to both a diffusive motion, which is described in the usual way by a Wiener process, and a directed motion, usually called a drift, which is given by the negative derivative of the potential field. It is readily shown that in the steady-state situation (i.e., when the probability distribution describing the particle's position has no time dependence), the probability of being at a location is related to the potential at that position. The largest probability for the particle's location occurs where the potential is smallest, or stated in visually evocative jargon, in the well of the potential field.

As a first approximation, the potential is assumed to depend only on the lateral position; it is assumed to act uniformly and instantly from the time the platelet crosses the entrance plane of the tube or channel. Only steady-state flows will be considered in this section, i.e., velocity and concentration profiles at all axial locations are independent of time. The physical events are assumed to be as follows: platelets enter the tube or channel from a stirred reservoir and are uniformly distributed across the entrance plane. As each platelet moves axially through the tube it also moves laterally because of the collisions and flow. These interactions are characterized by the potential and the random lateral motions; they redistribute the platelets to produce nonuniform concentration profiles. Sufficiently far downstream of the entrance, a fully developed state occurs. Here "fully developed" connotes that neither the velocity nor the concentration profile depends on the axial position; *it does not imply that the interactions or the lateral motions cease.* Throughout these events, each platlet is assumed to interact only with red cells, plasma, and the vessel surface. This is the assumption of diluteness; it implies that one platelet will not affect the motion of another. In the fully developed region, the distribution

of platelets reflects only the differences in rheological potential as different lateral positions. There, in any small length of tube, the axial convection delivers and removes statistically equal numbers of particles at each lateral location, and therefore, does not alter the overall particle balance. Because only the lateral position remains as an independent variable, there is a direct analogy between the platelet motions in the fully developed region of a steady-state blood flow and the stochastic problem involving the one-dimensional random walk of a particle in a potential field with wells.

The use of a potential to impose mechanical limits and conditions on a random walk is not novel. In modeling the Brownian motion of a particle in a pore of similar size to the particle. Brenner and Gaydos used a potential to describe the constraining effect of the cylindrical boundary on the motion of the particle (29). In contrast to their work, we are currently unable to describe the deterministic events in explicit mathematical terms, which reflects in part the less advanced state of concentrated suspension theory.

Estimation of the drift from the fully developed concentration profile

Because an explicit derivation of the potential is unavailable, we hypothesize that the potential is invariant over the length of the channel. (This hypothesis is discussed below.) If this is the case, the potential field can be determined to within a constant from a knowledge of the fully developed concentration distribution. For clarity, the derivation below uses an idealized channel flow of infinite width involving two-dimensional rectangular coordinates;[3] the y-axis measures the distance perpendicular to the wall, and the x-axis, a distance in the axial direction. Let $-\Phi'(y)$ be the local drift in the y-direction. (The prime denotes a derivative with respect to y.) Also, let J_y represent the flux of platelets in the lateral direction, D, the diffusion coefficient, assumed to be constant, and c, the local concentration. Then J_y can be written as:

$$J_y = -\Phi' c - D\partial c/\partial y. \quad (1)$$

It is common in the literature on stochastic processes to identify a probability flux similar to Eq. 1. In such equations c is replaced by the conditional probability for being located at a particular y position, given that the particle stated from a set position at a previous time (28).

Eq. 1 is readily solved for the special case when the velocity and concentration profiles are fully developed and in steady state. Then, there is no dependence of the concentration c upon x, and the above equation becomes an ordinary differential equation. Because the wall is impermeable and nonreactive, J_y equals zero there. Use of the conservation of flux relationship in a region extending laterally outward from the wall leads directly to the conclusion that J_y equals zero at all lateral stations. The solution of Eq. 1 then relates the steady state, fully developed concentration profile and the potential; it is

$$\ln (c_{fd}) = -\Phi/D + k. \quad (2)$$

Here k is a constant of integration and the subscript fd denotes fully developed. The drift $-\Phi'$ appropriate for the more general situation can be obtained from this relationship by chain-rule differentiation or by rearranging Eq. 1 after setting J_y equal to zero. In this initial work D is assumed to be a constant,[4] and the drift is

$$-\Phi' = Dc'_{fd}/c_{fd}, \quad (3)$$

where the prime denotes a derivative in the lateral direction. (The constant k is unimportant because it is lost in the process of differentiation.) The proportionality of the drift to the augmented diffusion constant is tied to interesting features in figures shown below.

Characteristics of the drift

Features of the drift can be graphically deduced from the experimentally determined concentration profiles. In particular, the derivative c'_{fd}, and hence, the drift, will be zero at the center of the channel (or tube) because of symmetry of the concentration profile; c'_{fd} is also zero at the peak because it is a maximum. These features can be observed in Fig. 1 *b*. The drift will have a relative maximum on the central side of the peak of c'_{fd} because c'_{fd} is positive on that side. The concentration profile immediately adjacent to the wall must be such that the drift term of the flux equation balances the usual diffusion term. (Descriptions of reaction at the wall surface require that the net lateral flux [given by Eq. 1] provide an amount equal to the rate of consumption by the reaction. Portions of the traditional diffusive flux term will then balance the vector sum of the drift and reactive consumption.)

[3]Equations for cylindrical coordinates are provided in Appendix A.

[4]With a variable diffusivity, the quantity $[-\Phi/D]$ can be determined from the steady-state concentration profile. Information on the parametric dependence of D would be sought from other experimental studies. An important point, relevant to later sections of the paper, is that the Stratonovich and Ito calculuses lead to the same stochastic differential equation when D is constant; this is not true for variable D.

Thermodynamic form

Nonuniform concentration fields occur as a part of mass transfer phenomena that involve movement of charged species in electrical potential fields. Such analyses use a formalism that demonstrates the extended flux equation from a thermodynamic perspective. Consider a descriptor that parallels the electrochemical potential, namely, $c \exp(\Phi/D)$, which is proportional to c/c_{fd}. With this descriptor the extended Fick's equation (Eq. 1) can be written as

$$J_y = -D \exp(-\Phi/D)\{d[c \exp(\Phi/D)]/dy\}. \quad (4)$$

The corresponding chemical potential, μ, is

$$\mu - \mu^\circ = RT \ln[c \exp(\Phi/D)] = RT(\ln c + \Phi/D). \quad (5)$$

Here, μ° is the chemical potential of the reference state, R is the gas constant and T is the absolute temperature. This form is consistent with an expected result: material moves down a gradient of chemical potential.

Through Eq. 5 we clearly see a premise accompanying the extended transport relationship for platelets, namely, the flow of a red-cell suspension in a channel or tube establishes and maintains the portion of the chemical potential that is described by Φ/D. In response to this induced potential, the concentration distribution is driven toward the form, $\ln c_{fd} = -\Phi/D$, which, when reached, establishes a condition of zero chemical potential at all lateral stations. Should the flow be disrupted, the rheological portion of the chemical potential, Φ/D, would change or disappear. Such an occurrence would establish an unsteady state where the excess platelets are available to react or disperse. Obviously, the closeness of the excess to the wall makes interaction with it likely.

Convective diffusion equation with potential terms

When the above concepts are used in a mathematical description of platelet transport in blood flow, some terms of the resulting transport equation are equivalent to those in the traditional convective diffusion equation (17). The shear-induced interactions cause an uncoordinated motion in the lateral direction that is modeled as a one-dimensional walk; its description uses an enhanced diffusion coefficient and a conventional Fickian expression for diffusions. For this derivation, axial diffusion/dispersion will be ignored. Due to the strong viscous stresses, which are characterized by a low-particle Reynolds number, it is assumed that immediately upon coming to a location, each particle assumes the axial velocity appropriate for that lateral location. Then, the axial flux is represented by the product of the local velocity and the concentration, which leads to traditional convective terms involving $\mathbf{U} \cdot \nabla c$. ($\mathbf{U}$ represents the velocity, assumed here to be an axially directed vector field.)

The steady-state extended convective diffusion equation (i.e., the one including potential terms) is readily generated by requiring the divergence of the flux to equal zero, i.e., $\nabla \cdot \mathbf{J} = 0$. The component $\mathbf{J}_y$ is given by Eq. 1 and

$$\mathbf{J}_x = \mathbf{U}(y)c. \quad (6)$$

The overall equation is

$$\mathbf{U}\partial c/\partial x = D\partial^2 c/\partial y^2 + \Phi'\partial c/\partial y + \Phi'' c, \quad (7)$$

which is readily recognized as an altered form of the traditional convective diffusion equation.[5] Note that although one Φ-related term has the mathematical form of a convective motion, it is not fully equivalent to a traditional convective term, such as that comprising the left-hand side of Eq. 7, because there is not a concomitant flux of red cells or plasma. Also note, that due to the form of Φ, each term on the right-hand side is proportional to D. An equation for the transient case can be obtained by using the form of the fluxes shown above and the customary approach involving conservation of material entering, leaving, and accumulating in a differential volume.

Peclét number scaling

An interesting scaled form of the equations occurs because of the nature of the potential. Let $x^* = x/\ell_x$, $y^* = y/\ell_y$, $u^* = \mathbf{U}/U_{max} = [1 - y^{*2}]$, and $c^* = c/C_0$, where ℓ_x is a characteristic length in the axial direction, ℓ_y is a characteristic length in the lateral direction, U_{max} represents the maximum speed of flow, and C_0 is a reference concentration. Then, the above equation can be written as

$$u^*\partial c^*/\partial x^* = \{D/U_{max}\ell_y\} \cdot \{\ell_x/\ell_y\} \cdot \{\partial^2 c^*/\partial y^{*2} - \partial[(c^*/c_{fd})(dc_{fd}/dy^*)]/\partial y^*\}.$$

As the tube extends along the positive x-axis, there is no natural measure of the axial dimension; accordingly, ℓ_x will be assumed equal to ℓ_y, which would be a channel half-height (or tube radius). The first group in braces on

[5]This simple situation will probably be lost upon dropping the assumption that the platelets are a dilute species.

the right-hand side is the inverse of the Paclét number ($Pe = U\ell/D$), which compares convective events to diffusive events. Taylor used a similar equation (there was no term involving c_{fd}) as an approximation of the dispersive motion in tube flow; he obtained the relationship that the axial dispersion is approximately $(Ua)^2/(48\ D)$ at high Peclét number (35). Turitto et al. constructed their measurements of the platelet diffusivity about this concept (14). Future work will explore whether the additional terms provide an improved model of Turitto's data at higher wall shear rates.

Relationship to multicomponent equations

The drift term is introduced in a single component platelet transport equation as a way to include more information about the events tied to the other phases (red cells and plasma). Because platelet transport is actually a multiple component phenomenon, it is reasonable to inquire about the relationship of the extended equation and conventional treatments of multicomponent mass transport. Analytical treatments of multicomponent transport phenomena (e.g., Hetsroni [30]) use a conservation equation for each component of the suspension. Each equation resembles a Navier-Stokes equation to fluid mechanics. The actions of components upon each other are described by interaction terms that are present in each of these equations. In blood flow, the minimum number of components to describe platelet transport is three: plasma (suspending fluid), red cells, and platelets. Due to their small size and relatively low number density, platelets are a dilute species. The flow is predominantly determined by the motions of the plasma and the red cells. The role of platelets in setting the velocity field for the flow is ignored in light of their minor contribution to the volume of the flowing suspension. Modeling of the bulk flow is assumed to be done separately, and, for the purposes here, to be adequately described by a Newtonian fluid. After that assumption only one equation remains, i.e., the one describing the motion of platelets. It includes, in addition to the convection by the bulk flow, actions of the plasma and red cells on the platelets in the form of an outside source, which we have chosen to model as a potential and an augmented diffusion.

Approximating the potential as axially invariant

The arguments of this paper have a circular nature: a drift function is determined from experimental estimates of a fully developed concentration profile to calculate a concentration profile. A sense of cause and effect is restored by judging the model according to its degree of success in predicting the axial development of the concentration profile. Because this development will be affected by the axial description of the potential, the reasons to invoke a fixed potential from the outset of the flow into the channel must be considered. For the in vitro experimental data this requires an understanding of the development of the velocity and red cell concentration profiles in blood flow from a well-stirred reservoir. The velocity events are relatively straightforward for flows with low Reynolds numbers; for this reason, only tubes or channels of small diameter or height are considered here and in the section on numerical modeling. The length to develop a parabolic velocity profile for the flow of a Newtonian fluid is well set (31). Significant near-wall excesses of platelets and platelet-sized bodies occur when the wall shear rate exceeds 200 s^{-1}, a condition where blood behaves approximately as a Newtonian fluid. The Reynolds numbers of our experiments in 200-μm tubes are < 10, which implies development lengths for velocity profiles on the order of a diameter. As a first approximation, it is reasonable to ignore this short distance and treat the blood flow as instantly achieving a parabolic profile at the entrance. Assuming a Newtonian fluid obviates the issue of relative separation of the red cells and plasma since, by definition, a Newtonian fluid is a single entity that cannot separate. Observations of blood flow in small tubes show that a marginal layer develops essentially upon entry into the tube but that slow development of the red cell concentration profile and of the distribution of red cell orientations continues over many centimeters (32, 33). Such events are ignored in this first attempt to extend the platelet transport equation. For this case (fully developed, steady-state velocity profile and incompletely developed concentration profile), the events causing the mechanical portion of the chemical potential are constant along the axial length. Each of the aforementioned red cell effects can probably be included as a correction or improvement, with the concomitant complication that the drift loses its axial invariance.[6]

[6]If the drift were to vary axially, it would seem reasonable that it is zero at the entrance, quickly becomes large near the wall, especially in the region of high shear rate and variable RBC concentration near the wall at the entrance, possibly overshoots the potential associated with the fully developed distribution, and then decays to the value associated with the fully developed distribution. The acceleration at the entrance, with its extensional strain rates, may also produce an outwardly directed drift of platelets.

Stochastic differential equations: the dual view

The equations shown in this section allow the particle to be tracked during its motion through the tube or channel. Stochastic differential equations are a natural approach since they combine random and directed parts, just as the motion is a sum of such parts. The changes of lateral location are described by a drift term and a random-walk term, namely by

$$dy = \Phi'(y)dt + dG_y(t), \tag{8a}$$

where Φ' is the drift, y is a stochastic process representing the lateral location, and $d\mathbf{G}_y$ is a restricted Gaussian process with the average property $\langle d\mathbf{G}_y(t)d\mathbf{G}_y(t')\rangle = 2D\delta(t - t')$, where D is a diffusion coefficient, and δ is the Dirac delta function. The equal weighting of each term on the right-hand side of Eq. 8a by the factor D is not as obvious as in Eq. 7. However, Eq. 8a clearly shows that the drift acts as a position-dependent biasing factor in the random walk. The walls restrict the random walk by virtue of their impenetrable condition, i.e., the action of reflecting the particle from the wall. An important point deduced from this observation is that because $\mathbf{G}_y$ is not a Gaussian noise, y is a non-Gaussian, Markov process; this aspect is discussed by Van Den Broeck (34).

The changes of axial location are described by a convective motion, and, if axial diffusion is modeled, a random walk term, i.e., by either

$$dx = \mathbf{U}(y)dt \tag{8b}$$

or

$$dx = \mathbf{U}(y)dt + d\mathbf{F}_x(t), \tag{8c}$$

where

$$\langle d\mathbf{F}_x(t)\, d\mathbf{F}_x(t')\rangle = 2D\delta(t - t').$$

Here, x is an axial position, $\mathbf{U}$ is a function describing the axial velocity, which is solely a function of the lateral position, and $d\mathbf{F}_x$ is a Gaussian noise (Wiener process). Note that since the above equation for x involves y, which is a stochastic process, x is also a stochastic process, if Eq. 8c is used, then x and y are independent stochastic processes. As before, the drift would be obtained from the steady-state concentration distribution and the potential/drift would be assumed to act from the beginning of the channel. If the process of Taylor diffusion is to be simulated completely, Eq. 8c is chosen over Eq. 8b (34). Another choice is to ignore the axial diffusion terms, as Taylor did in his original physical argument regarding flow-induced dispersion (35), and use Eq. 8b. The relative scales of axial and lateral motions are set for the simulation by use of a Peclét number. That scaling is apparent for Eq. 8c because D appears in the definition of $d\mathbf{F}_x$ and $\mathbf{U}$ appears in the main equation; it is less obvious for Eq. 8b, where D enters because of the random motion depicted in Eq. 8a.

The approaches described by Eq. 7, 8a, and 8b form a duality. Gardiner (28) shows the relationship between the stochastic differential equation for the motion of a Brownian particle in a potential field and the dual Fokker-Planck equation, which describes the conditional probability of finding the particle at any location given that it started at the same location as was used for the origin of the stochastic differential equation. The Fokker-Planck equation underlying Eq. 7, the extended convective diffusion equation, describes the history of an ensemble of particles that all begin at the entrance plane of the tube. Each member of the ensemble could also be tracked by the stochastic differential equations of the evolution of the probability distribution describing particle locations could be tracked by the Fokker-Planck equation. The net outcome would be the same. These equations parallel the well-known duality of the diffusion equation and the Langevin description of Brownian motion.[7]

NUMERICAL STUDIES

Studies of the development of the concentration profile offered a way to investigate the consistency of the model, as represented by the above equations, with the experimental data. Numberical methods were used because explicit analytical solutions of the above equations were not available. Aspects described below include an equation that models the potential/drift, particulars related to the finite difference program used to evaluate Eq. 7 in the developing region, and methods for a simulation program that follows the rules codified by Eq. 8 and extended to describe deposition of material on a wall.

[7]Readers acquainted with stochastic processes will appreciate that the presentation here (Eq 8) parallels the Schmoluchowski approximation of Brownian motion. A more complete description of platelet motions could be made using lateral position and lateral velocity as stochastic variables; the arguments would be similar to those used in the Ornstein-Uhlenbeck description of Brownian motion (28). Such a treatment would involve discontinuities in the lateral velocity (instead of in position), which has more appeal on a physical basis. However, the mathematics is more complex, and the approximation used here appears to be adequate to describe the available data.

Drift/potential models

A description of the drift or its integral precursor, the potential, was needed to implement the concepts presented above. The numerical studies below were based on a functional form that provides a visually pleasing approximation to the observed concentration profiles.[8] Several functions (beta, exponential, power functions) were found that had the appropriate properties (see above) and that would mimic the shape of individual experiments. A beta function was used to obtain the profiles shown below; that function was

$$c = C_0 [1 + KR^{(m-1)} (1 - R)^{n-1)}], \quad (9)$$

where R was the relative lateral position (i.e., distance from the center divided by channel half-height or radial position divided by tube radius), K was a parameter that set the relative amplitude of the shape, C_0 was a normalizing parameter, and m and n were the exponents of the beta function. To produce the effect of a near-wall peak added to a uniform concentration, m was made large and n was set at 2. With this value of n, the concentrations at the wall and in the center were equal in the fully developed concentration profile. The peak occurred at a relative lateral position given by $(m-1)/m$. The value C_0 was selected so the axial flux in the fully developed region corresponded to a flow from a uniform reservoir having a concentration of one. The axial flux was $A = \int c\mathbf{U} \cdot \mathbf{da}$, where **da** is the area element appropriate for the geometry, i.e., a channel or tube. All computations used a parabolic velocity profile as an approximation for the slightly blunted profile that is known to occur in blood flow through small tubes (19).

The fully developed concentration profile and drift relationship as predicted by Eq. 9 are shown in Fig. 1, *a* and *b*. Comparison of the profile shape with published concentration profiles shows that the function captures the general features of the experimental data. Using the width of the near-wall excess as the main criterion, the function is appropriate for a tube with an inner diamter of ~100 μm. Profiles for larger tubes would have to use a larger value of m to limit the distance which the excess extends from the wall. In part, the decision to calculate profiles with $m = 19$ reflects the need for finer finite difference meshes to calculate profiles with higher values of m. Unless otherwise mentioned, the parameters for the curves illustrated in Fig. 1 are pertinent to other figures throughout the paper.

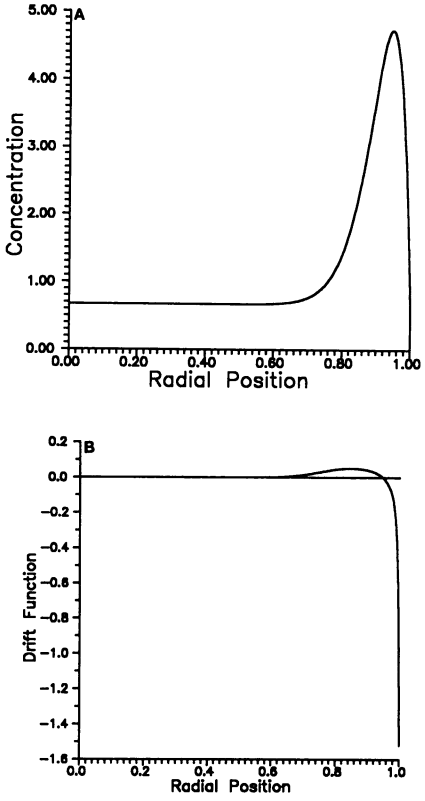

FIGURE 1 Functions to mimic the relative concentration profile and drift functions. (*A*) Eq. 9 is shown for $m = 19$, $n = 2$, and $K = 0.8 \cdot m(m + 1) = 304$; C_0 is chosen so that the inlet flux (assuming a parabolic velocity profile) is one. This convention produces a reservoir concentration equal to one vertical unit. The abscissa represents the relative lateral (radial) position, with zero being the centerline and one, the wall. (*B*) The drift function as calculated with the concentration profile illustrated in *A* and with a value of $D = 1.25 \cdot 10^{-7}$ cm²/s; the vertical scale has units of 0.0025 cm/s. The abscissa is, as in *A*, a relative lateral location. These profiles would be appropriate for a tube with an inner diameter of 100 μm and a flow with a wall shear rate > 400 s^{-1}.

Finite-difference model

Calculations of concentration profiles in the developing region of the tube used a finite difference method to solve a version of Eq. 7 appropriate for a cylindrical geometry; a transformed equation incorporating the thermodynamic form was used. (Appendix A outlines the derivation and shows the equations.) Use of the thermodynamic form of the potential/concentration (Eq. 4) was convenient because it resulted in an equation

[8]The first attempt to describe the potential involved fitting orthogonal polynomials to experimental data. The results were unsatisfactory, as judged by carrying the process "full circle," i.e., the fully developed platelet concentration profile calculated from a fitted potential did not closely resemble the initial experimental profile. The failure of the fitting process was attributed to error accumulation due to the use of a limited number of numerically fit terms, when in fact a larger number of terms or an infinite series may be needed to fit the data.

with one less term than the direct equation for tubular flow.[9] Boundary values were obtained by imposing conditions of symmetry at the center and of no total flux at the wall (i.e., $J_y = 0$, see Eq. 1); the condition at the entrance was that of a uniform concentration arbitrarily set at one. Initial efforts to numerically evaluate this equation were unsuccessful because the axial mass flux calculated at downstream locations differed substantially from the axial mass flux at the entrance. Such problems and methods for limiting their effects have been reported by other workers (36–38). To control this mass balance error, a Lagrange-style stabilizing term was added to the transformed version of Eq. 7. (For details of this method, see 37, 38.) The stablizing term involved conservation of mass flux in the axial direction, namely,

$$\mathbf{g} = A - \int c\mathbf{U} \cdot \mathbf{da}, \tag{10}$$

where **da** is the area element appropriate for the geometry (either tube or channel) and the quantity A is the flux at the entrance. Note that $\mathbf{g} = 0$ when the flux through a particular axial location equals the inlet mass flux. Following the concepts cited (37, 38), the enlarged equation to be solved numerically was

$$\nabla \cdot \mathbf{J} - \lambda \mathbf{g} \cdot \nabla \mathbf{g} = 0. \tag{11}$$

Selection of values for the coefficient λ is discussed by Hochfield (37). For a channel flow a value of one was used, whereas for a tube flow a value of $1/\pi$ was used.

Standard finite difference approximations of this equation were programmed. Eq. 11 was discretized after an implicit (Crank-Nicholson) method for the lateral direction and an explicit method for the axial direction. Without the **g** term the finite difference equations would have a banded diagonal matrix. Due to the definition of the **g** term the matrix is fully populated, but there are relatively small terms for the nontridiagonal elements. To solve this system without tackling the full matrix, an iterative approach was adopted. The first attempt to estimate the next downstream row of values used the upstream row of values to estimate all the **g**-related terms. The second and subsequent attempts to calculate the downstream row of values used the previous estimate of the downstream values to calculate the **g**-related terms for the downstream row of values. (The upstream, known row of lateral values was used in each iteration.) This approximation of the **g**-related terms results in a traditional tridiagonal matrix formulation. The iterative process was repeated until there was <0.00001 difference between any of the last estimated and the recently calculated downstream concentration values. Up to 1,024 steps (Δy) were used in the lateral direction; the number of steps (Δx) in the axial direction was chosen to satisfy the stability criterion, $(D\Delta y/U_{ave}\Delta x^2)$. Because the stabilizing term involved all points on the finite difference mesh, an iterative method was used to obtain each new set of downstream points. The drift function was set at above; it corresponded to a 100-μm tube radius. A parabolic axial velocity profile with an average speed of 1 cm/s was used. Values of augmented diffusion coefficient from 10^{-8} to $5 \cdot 10^{-6}$ were used in the model. Profiles were collected when particular concentration values occurred at the lateral position that corresponded to the position of the peak in the fully developed concentration profile. The lateral position of the fully developed peak, the concentration there, and the fully developed concentration profile were respectively denoted by r_{fdp}, $c(r_{fdp})$, and $c_{fd}(r)$. Specifically, profiles were recorded the first time the calculated concentration at r_{fdp} was $c(r_{fdp}) \geq 1 + n\%[c_{fd}(r_{fdp}) - 1]$. For the set of profiles shown in Fig. 2, n was 5, 25, 50, 75, or 100. The heights of peaks of the profiles in Fig. 2 are proportional

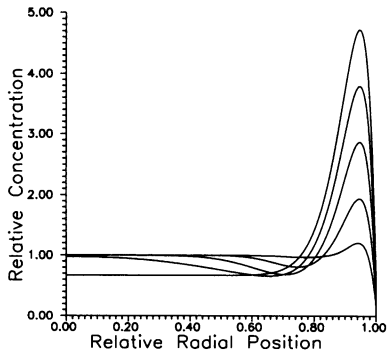

FIGURE 2 Concentration profiles calculated with a finite difference program. The method used to select profiles is discussed in the text. Parameters for the drift are as shown in Fig. 1.

[9]Transformation changes the nature of the equations; the untransformed equation, Eq. 7, is quasi-linear, while the transformed equation, Eq. A3, is linear. (However, adding the stabilizing term again makes the equation quasilinear.) Also, the shape and nature of the concentration fields differs for the untransformed and transformed equations. In the solution for the untransformed relationship, the concentration near the wall at locations further downstream rises above the initial value, while in that for the transformed solution, the concentration near the wall at locations further downstream becomes closer to the uniform condition. This is easily visualized since the transformed equation in c/c_{fd} has a well at the lateral location of the peak in the untransformed fully developed concentration profile. Because of this behavior, the Fokker-Planck equations corresponding to untransformed and transformed equations are occasionally referred to as classified as forwards and backwards relationships (28).

to the precentage value, e.g., the profile for 25% is the one with the second shortest height.

Examination of Fig. 2 shows that most profiles have peaks that are centered on the position of the peak in the fully developed concentration profile, r_{fdp}, suggesting a picture of entrance events wherein the major outcome of the drifting motion is the collection of material in the well. A close examination of profiles from the entrance up to the axial location for the profile with a peak having 5% excess concentration showed that a small peak occurs between r_{fdp} and the wall. This occurrence is probably a manifestation of the high inward drift in this region. After the peak centers on r_{fdp} it remains there. For each profile, there is region of relatively low concentration between the center and the peak; in this region the drift is sufficiently strong to create a local depletion, which is filled from the central convective stream by a combination of drift and diffusion. In a simplistic sense, this region is the source of the "excess" material that forms the peak. When profiles are collected by the above rule, they are true for arbitrary values of the diffusion coefficient. This occurs because both the rate at which material moves toward r_{fdp} and diffuses away from r_{fdp} are proportional to D. Because the drift is negligible in the central region, the diffusive motion is the primary means by which particles make their way from the center to the dip where there is significant drift.

The Peclét-number scaling shown above illustrates that the axial development of peak height is dependent upon the group Ux/D. Fig. 3 shows $c(r_{fdp})$ as a function of axial distance for several values of D from $1 \cdot 10^{-7}$ to $5 \cdot 10^{-6}$ cm^2/s and U_{ave} = 1 cm/s. An effect of the Peclét number scaling is that, for fixed U_{ave} and diameter, the

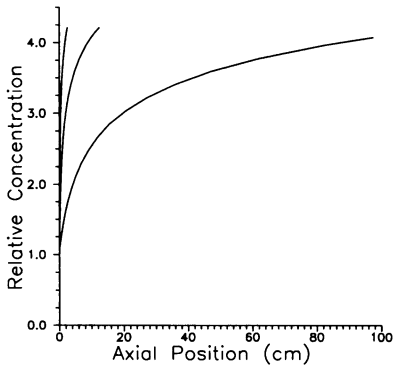

FIGURE 3 Curves showing the concentration at the radial position of the peak in the fully developed concentration profile. For the left curve, $D = 5 \cdot 10^{-6}$ cm^2/s, for the middle curve, $D = 1 \cdot 10^{-6}$ cm^2/s, and for the right curve, $D = 1 \cdot 10^{-7}$ cm^2/s; all other parameters are as in Fig. 1.

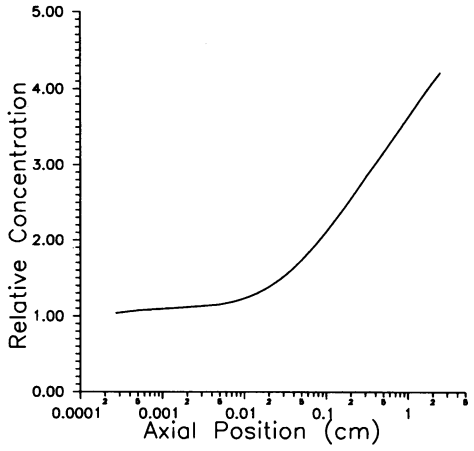

FIGURE 4 Relative concentration vs. logarithm of axial position. The abscissal units are centimeters; for the curve shown, U_{ave} = 1 cms and $D = 5 \cdot 10^{-6}$ cm^2/s.

distance to reach a given concentration decreases as the diffusivity increases. The rapid growth of the peak observed for the larger diffusivities is consistent with the experimental data. To illustrate the approach to the fully developed profile, in Fig. 4 the data of the previous figure are plotted semilogarithmically. A noteworthy feature of this plot is the special region where growth is approximately linear. What occurs beyond this point could not be investigated numerically due to instabilities in the iteration process. A physical argument for asymptotic final growth is that the material in the center must diffuse to the region of higher drift. Because this diffusive motion must occur with less and less concentration difference to drive the motion, the growth process will slow with distance.

Simulation

Using stochastic differential equations shown above, a program was developed to simulate the freeze-capture experiments which were used to determine concentration profiles of platelet-sized latex beads in flowing red cell suspensions (7–9). In those experiments, a steady-state distribution of material in the tube was established; then, the tube and its contents were rapidly frozen to capture the positions of the latex-bead platelet analogues. Concentration profiles were determined from microscope measurements of particle positions on cross-sectional surfaces of frozen tube.

The equations that were simulated (Eq. 8) corresponded to taking steps in the lateral and axial directions. Particles that reached the wall and that crossed

the centerline were reflected back across those boundaries; this treatment corresponded to having no flux through the wall and a zero concentration gradient at the center. Because the particles did not interact (dilute approximation), each particle's trajectory was simulated individually. For tube flows, an explicit (or direct) simulation was used. To calculate the step in the axial direction, the instantaneous lateral position was used to determine the axial velocity, which was multiplied by the time increment, τ. Each step in the lateral direction had a contribution from both the drift function and a random number generator. The Box-Mueller approximation was used to convert values from the uniform random number generator of the computer language (TurboPascal 5.0, Borland) into a (0, 1) normally distributed random number sequence. Individual numbers from this sequence were multiplied by $(2D\tau)^{1/2}$ to obtain the diffusive steps. Drift steps were given by the product of the time step and the value of the above described drift function appropriate to the particular lateral location. The program mimicked the continuous inflow by starting the simulations of batches of particles at instants of time separated by the increment, τ. The particles comprising each batch had a maximum time of simulation; those times were $M - \tau$, $M - 2\tau$, $M - 3\tau$, ... (Note that M was selected to be a multiple of τ.) Zero time corresponded to the time at which the tube was frozen.

For some channel flow simulations, Eq. 8a,b were numerically approximated by a collocation technique (39) that is more accurate for a given size of τ than an explicit simulation. The occurrence of similar profiles with programs using the collocation and explicit techniques and the lack of change of profiles when they were calculated using smaller time steps in the explicit program were taken as ex post facto indications that calculations with the explicit method and the chosen size of time step provided reasonable estimates. The particles of each batch were started at lateral positions selected so the condition of uniform flux at the entrance would be approximated. Two methods of assigning initial location were used: randomly under the appropriate distribution function and deterministically to appropriate average radial locations; no difference of average outcome was observed. For a valid simulation, the maximum time of simulation, $M - \tau$, had to be large enough that a condition of steady state was mimicked by the time at which "freezing" occurred. The value of M used for the numerical experiments, 25 s, was such that all the particles for the initial few batches and most of the particles in the initial third of the batches passed through the region of interest. The remainder of the particles would be captured by the "freezing" process which occurred when time expired.[10] When a particle's trajectory carried it beyond the furthest sampling zone before the clock expired, it was ignored. Such particles corresponded to those experimental particles that would wash through the tube and could not be trapped by the freezing process. The time step τ was set as $\tau = (\ell/[sU_{max}])$, where ℓ = distance from the entrance to the last point of the furthest zone that was frozen, U_{max} = the maximum axial speed, and s was a parameter that set the minimum number of diffusive steps to move through the tube for a particle on the fastest streamline. This parameter was set at 100, a value chosen after noting that simulations with $s = 200$ had the same profile shapes as those for $s = 100$. The simulations used the drift function illustrated in Fig. 1. A simulation with a D of $1.25 \cdot 10^{-7}$ cm^2/s was run; other specific values were $U_{max} = 2.0$ cm/s, $R = 0.005$ cm, $\delta/R = 0.02$ (δ represents the platelet radius), $\tau = 0.05$ s, and $M = 25$ s, which mimics events in 100-μm tubes.

Freeze-capture experiments derive concentration profiles from many cross-sections of short lengths of tube (generally <5 mm). Unless an unwieldy number of individual simulations were done, this aspect could only be simulated crudely. For this reason, particles were counted as being captured "at" a given axial station if they were within ± 0.25 cm of the station at time zero, e.g., everything from 2.0 to 2.5 cm was counted as being at 2.25 cm. For each axial segment of simulated "frozen" tube, the output was a list of lateral positions at which particles were captured by the freezing process. As was done with the experimental data, a kernel estimate technique was used to estimate the concentration profile from these data (40, 41). The frequency distributions estimated from the simulation output were converted to concentrations relative to the reservoir concentration using a conservation of mass expression that assumed a parabolic velocity profile for the tube flow.

Resulting profiles for half centimeter sections ending 5 cm from the entrance are presented in Fig. 5. The estimated concentrations in the center of the tube were erratic because only a small number of simulation points were obtained per increment of the radius there; for this reason, no concentrations are shown for a relative radial position <0.2. The relative amplitudes of the profiles generally agreed with those predicted by numerical

[10] M is finite because the simulation is for suspended particles and not for the suspending fluid. The slowest axial speed and, hence, the maximum time needed for a simulation were small finite values because the particles were not allowed to "stick" to the wall and because the particles had a small, but nonzero size. No extra drag or interaction with the wall (beyond that included as a part of the drift) was included.

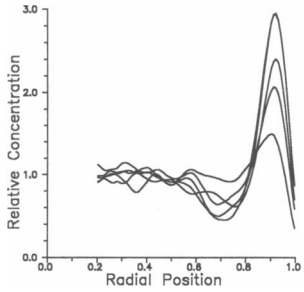

FIGURE 5 Concentration profiles from a simulation of the freeze-capture experiments; parameters are as in Fig. 1. Profiles are in order of ascending peak height for section 0.5–1.0, 1.5–2.0, 2.5–3.0, 3.5–4.0, and 4.5–5.0 cm. from the entrance. The last two profiles have essentially the same peak amplitude.

integration of the field equation. An obvious advantage of the field equation over simulations is that calculations with it produce smoother profiles. Because the simulation and finite difference methods are subject to different errors, the similarity of outcomes suggests that the numerical picture of profile development is free from gross errors.

Reaction at a surface: maintenance of the near-wall excess

How the drift affects deposition on the wall is of great interest. Analysis of the traditional convective diffusion equation leads to the observation that at low to moderate wall shear rates, platelet deposition is limited by the process of delivering reactants (particles) to the surface (17, 19, 20). It also shows that for surfaces with low rates of reactivity (as compared to the rate of delivery), the concentration profile is minimally changed. A similar situation should occur for the extended transport equation. For surfaces with low reaction rates, the profiles will be much like those of Fig. 2 since the reactive consumption cannot greatly change the numbers of nearby platelets. This seemingly innocent event may have important consequences. Consider that the extra platelets are in the peak which is only slightly off the wall. Calculations of the amount of agonistic material (thrombin, ADP) released by upstream platelets suggests that significant concentrations of these materials would occur in the region of the peak (42, 43). Such exposure could lead to enhanced downstream deposition. It is possible that this would explain reported results for elevated deposition onto collagen at downstream locations when the wall shear rate is high (44).

Another interesting case involves surfaces with very high reaction rates, which was investigated by modifying the simulation so that particles could be deposited on the wall. The method of simulations was chosen because numerical solution of the transient finite difference equations would have required much greater computational effort and also because the simulation implementation of boundary conditions involving conditional deposition. Three sets of reaction parameters/boundary conditions were chosen to illustrate the events associated with deposition. In two simulations (*A* and *B*), the first time each particle reached the wall, it deposited; this condition should mimic an infinite capacity for reaction at the surface. Simulation *A* included a drift term; simulation *B* did not. In the third simulation (*C*), each time a particle would interact with the wall, it had a 50% chance of depositing. Once deposited, a particle had a 10% chance of leaving on the next time step. The particle was permanently deposited when it had accumulated a total of 10 events, an event being the initial deposition on the wall, a redeposition on the wall, or the condition of remaining deposited during a time step of the simulation. The profiles that resulted from these simulations are shown in Fig. 6 *A–C*. As expected, profiles from the simulation without drift, Fig. 6 *B*, had no near wall excess. Both simulations with drift exhibited profiles with near-wall excesses; this was true even for Fig. 6 *A*, where the reaction rate was effectively infinite as compared to the delivery rate. As the reaction (deposition) requirements were relaxed, the peaks of the near-wall excess became higher, (Fig. 6 *A* and Fig. 6 *C*); a rationale for this was presented above. These profiles were consistent with the interpretation that blood flow induced a drift, which attempted to accumulate all the tracer particles at a location near the wall, but that such an accumulation was limited by either diffusion back into the core flow or diffusion to the reactive site.

The simulation program with deposition was constructed so that it counted the numbers of tracer particles that were deposited at various axial zones, each 1 cm long, along the tube. The relative amounts of axial deposition for the three sets of deposition parameters are illustrated in Fig. 6 *D*; the letters used above to identify simulation conditions are also used to mark the corresponding curves. Simulation B, the case without drift, showed a great decrease in the amount deposited at downstream axial zones; this outcome was consistent with the decreasing concentration gradients shown in Fig. 6 *B*. Simulations *A* and *C*, cases which included drift, illustrated that drift increased the overall amount of deposition. This occurred despite the fact that the drift immediately adjacent to the wall acted to move particles away from the wall. The increased deposition can be ascribed to the drift-induced near-wall peak which establishes a greater concentration gradient than would exist if there were no drift. Interestingly, after the

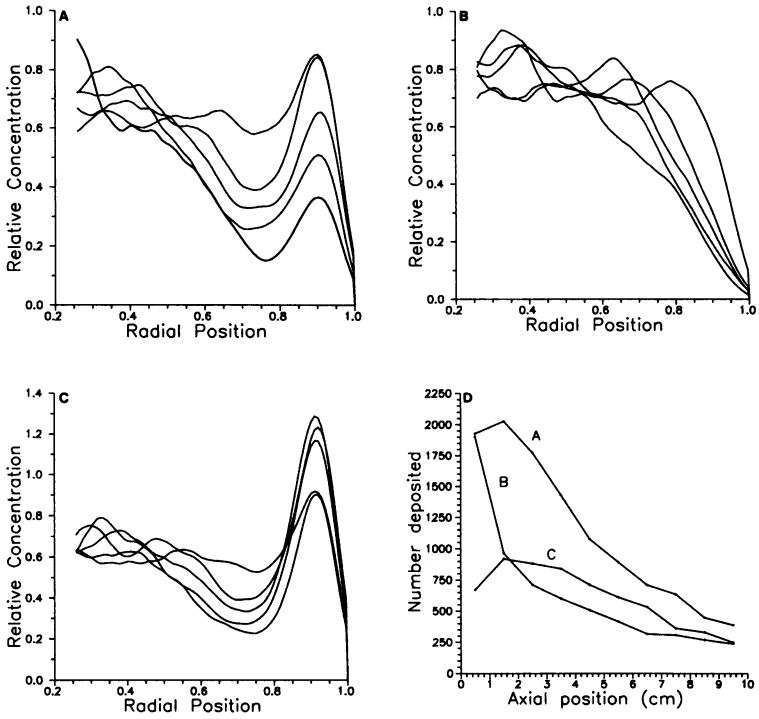

FIGURE 6 Results of simulations that included deposition on the wall. All simulations used $D = 1.25 \cdot 10^{-7}$ cm^2/s. Profiles shown in *A* were calculated using the drift depicted in Fig. 1 and a condition that, upon reaching the wall, all particles wall deposited permanently. The distances from the entrance to the middle of the zone in which particle positions were collected are, in order, corresponding to increasing heights of the near-wall peaks of the curves at r_p (a relative radial position 0.93): 8.5, 6.5, 4.5, 2.5, 0.5 cm. *B* is for the same deposition rule but without drift ($K = 0$); note that no excess occurs, and that as expected from conventional mass transfer theory, the near-wall slope tends to be less for profiles taken further downstream. The distances from the entrance to the middle of the zone in which particle positions were collected are, in order, corresponding to increasing slope of the profile at the wall (realtive radial position = 1.0), 8.5, 6.5, 4.5, 2.5, 0.5 cm. Profiles of *C* are for the same drift function as in *A*, but the chance of adhering to the wall is less, 0.5, with additional conditions explained in the text. The distances from the entrance to the middle of the zone in which particle positions were collected are, in order, corresponding to increasing height of the near-wall peaks of the curves at r_{fdp}: 8.5, 0.5, 6.5, 2.5, 4.5 cm. (Profiles for stations at 8.5 and 0.5 cm have virtually identical peak heights.) Note the occurrence of relative peaks in the profiles for *A* and *C*. *D* Curves for each simulation illustrating the number of particles deposited on centimeter-long axial segments of tube wall. The number deposited in each segment is plotted versus the distance from the entrance to the mid point of the segment in centimeters. Curves *A*, *B*, and *C*, respectively, correspond to situations described in parts A, *B*, and *C* above. Each simulation had 50,000 particles entering the tube.

initial consumption of near-wall platelets in the first axial zone, the moderate reaction conditions, which were chosen on an *ad hoc* basis to mimic some reported features of thrombogenesis, had approximately the same deposition as the no-drift case with strong reaction conditions.

Discussion

The accumulation of a near-wall excess is a simple example of self organization in an open system.[11] The organization demonstrated in the platelet concentration profile is produced by the flows of energy and material through the system. For a suspension such flows are accompanied by jostling, tumbling, and colliding events among the particles. Such events force each tracer particle (platelet) to explore the potential field *and* are the origin of the augmented diffusive motion. This connection to basic rheological events makes it reasonable that the average movement toward wells in the potential field is proportional to the effective diffusion coefficient. Over a sufficiently long path in the fully developed region (or equivalently, total time spent in the region), the proportion of time spent at each lateral location will be proportional to the concentration there. In the sense that the statistical distribution for the fully developed state is fixed from the outset, the set of biased motions of the tracer particles is determinate. It is

[11]The term "open system" is used in the thermodynamic sense to connote a region whose boundaries are defined by the walls and cross-sectional planes across the tube or channel.

crucial to note that the concept is *not* that a particular particle will move directly to a specific position.

Although the potential/drift is not calculated directly from primary events, its shape and size permit sensible speculation about the causative basic events. The primary event in the region very close to the wall is the physical and fluid mechanical repulsion that suspended particles experience as they flow past a wall. Such repulsions are the probable reason why the peak of platelet concentration does not occur directly at (on) the wall and why the drift has an off-wall direction in the region immediately adjacent to the wall. It is known that in dilute solutions there is a more rapid off-wall motion of larger bodies than smaller bodies; also, flexible bodies move further and more quickly than rigid bodies. These observations suggest that because of size and flexibility, red cells will be preferentially excluded from the near-wall region (as compared to platelets). The repulsion of red cells from the wall is limited by their accumulation in the center. The shearing motions of the flow prevent the red cells from being packed in the central region; stated positively, the shearing motion acts to expand the red cell suspension. (Bagnold demonstrated and measured the normal force that is exerted when a suspension of rigid particles is sheared in a Couette apparatus [45].) These competing events control the size and nature of the marginal layer and its red cell distribution. Bugliarello and Sevilla showed that the height of the peripheral plasma layer is variable and must be viewed in a statistical sense (27). Indirectly, this suggests that the concentration of red cells in the marginal layer should be viewed in the same way. The region of increasing local hematocrit would be expected to extend from the wall a distance corresponding to several RBC diameters (20–30 μm). A region of this size includes most observed incidences of the near-wall excess; the only know exception is a work by Aarts et al., (2) who report a size about an order of magnitude greater.

The events in this special near-wall region will be of two types. Very close to the wall, platelets can be expected to be physically and fluid mechanically repelled from the wall. This region would extend for two or more platelet diameters. Beyond this, the wall repulsive events exerted on platelets are expected to be minimal. However, the collision process will still be influenced by the distribution of red cells. Seitz (46) shows that there is a net flux from a region of higher collision rate to a region of lower collision rate. The gradient of red cell concentration near the wall that exists in a shearing flow establishes such a region of variable collision rate. This is the origin of the drifting toward the wall. This concept was outlined previously (47) and referred to by the somewhat whimsical title of rheophoresis. Note that neither viewpoint attributes the motion of platelets toward the wall because of their exclusion from the center (being forced out from the center by the incoming red cells). That viewpoint is incompatible with the observation of large near-wall excesses of platelets or beads at relatively low hematocrits (15–25%).

As the expression for the drift function is an approximation, only qualitative comparisons of calculated and experimental concentration profiles will be made. The numerical experiments show that a peak develops quickly, but that the complete shape develops more slowly. Calculations show that the distance required to reach a given concentration at the lateral position of the peak is smaller for larger diffusion coefficients and larger for larger mean convective speeds. After careful review of the experimentally determined concentration profiles, it is clear that what had been taken as full development (8, 48) could also be taken as the end of the rapid early development. If this is the case, the drift function would have a larger amplitude and perhaps a slightly different shape. Due to the nature of the measurement process, i.e., the collection of many position measurements from which a distribution is estimated, the peak amplitude in the experimental profiles are of limited accuracy. Improved accuracy would require obtaining many more samples from individual trials, and each sample would have several thousand position measurements. This task would be complicated by the occurrence of significant sample to sample variation in the shape of the concentration profile. While the near-wall excess occurs regularly and is substantial, its height is quite variable (±30%). The dip that is observed on the central side of the peak of calculated profiles is also of interest. Such a dip is present in many of the experimentally determined profiles with a near-wall excess. However, obtaining direct confirmation of this dip is also difficult because of the limited resolution of the experiments.

The next stages of developing the extended equation are to consider the effect of variable diffusivity, to include entry regions for development of velocity, hematocrit, and RBC orientation profiles. These extensions correspond to relaxing the axial invariance of the potential and accounting more correctly for shear-induced suspension events (collisions) that depend upon the local values of shear rate and the hematocrit. It would seem that the viewpoint presented here, that of separating the motion that results from the collisions into determinate and random parts, will remain a useful approach. Whether the amplitude of the drift will retain its simple proportionality to the diffusion coefficient is less clear. As noted earlier, the random motions force the particle to explore the potential field and find the wells. It is reasonable to expect that a low diffusivity in the central region of the flow will effectively trap platelets there, and they would be forced to move with

the axial convective motion. Such a scenario is consistent with the existence of a dip located on the central side of the near-wall excess in the concentration profile. If, as commonly done, the diffusivity is assumed to be proportional to the wall shear rate, the ratio of D/U_{max} will not depend on shear rate.[12] Modifications would still be needed to include the radial and axial variations of hematocrit. Waters' studies (8, 44) of the profile at three different axial locations (0–1 cm, 10–11 cm, and 30–31 cm from the entrance) showed that the amplitudes of the near-wall excesses of the 10–11 and 30–31 cm tube segments were statistically indistinguishable for shear rates of 400 s^{-1} and higher. When the wall shear rate was low (100 and 200 s^{-1}), the peak amplitudes were higher for the 30–31 cm tube segments. A minimum level of shear rate may be necessary to have deformation of the red cells and the concomitantly high diffusivity required to observe concentration profiles with large near-wall excesses within short distances of the entrance.

The use of a potential term in the model is workable approximation, but an incomplete answer. With it, a simple one-component transport equation can be used to describe concentration profiles in the physiologically most common geometries (tube and channel). Given the difficulties connected with using general multicomponent equations, this capability is important. The extended equation can be used in blood transport/mass transfer problems much like assumed velocity profiles are used in predictions of turbulent mass and heat transfer. The truly complete solution, the direct prediction of the potential from the mechanics of the many interacting particles, remains as a challenge. Its availability would allow the use of this concept for more complex flow geometries.

CONCLUSIONS

The introduction of a potential term into the transport equation for platelets allowed a mathematical description of the near-wall excess. Due to its means of definition, the potential automatically reproduced the fully developed concentration profile when there was no reaction or loss of material. Using analytical forms that approximated the observed concentration profiles, numerical studies of the extended convective-diffusion equation were done; the studies used typical values of the augmented diffusion coefficient. The results showed that the peak of the near-wall excess developed in a short length, which was consistent with the experimental data. They also showed a continued slow growth of the peak toward the fully developed profile. These numerical experiments were corroborated by direct simulations based on the equivalent set of stochastic differential equations. Simulations of tube flow with deposition on the walls indicated that the inclusion of a drift phenomenon will enhance the amount of deposition.

[12]Zydney and Colton (22) provide a thoughtful, thorough review of data illustrating the parametric dependence of shear-augment dispersion.

APPENDIX A

Equations for the cylindrical case

Let

$$\underline{C} = c \exp\{\Phi/D\} \text{ and } \underline{D} = D \exp\{-\Phi/D\}.$$

Then

$$Jr = -\underline{D}\,\partial\underline{C}/\partial r \tag{A1a}$$

and

$$J_z = U\underline{D}\,\underline{C}/D, \tag{A1b}$$

where U is the parabolic velocity profile, $U = U_{max}\{1 - (r/R)^2\}$. Using conservation of species, expressed by

$$\nabla \cdot \mathbf{J} = 0 = J_r/r + \partial J_r/\partial r + \partial J_z/\partial z,$$

we obtain

$$U\partial\underline{C}/\partial z = D\partial^2\underline{C}/\partial r^2 - [\Phi' - D/r]\partial\underline{C}/\partial r. \tag{A2}$$

The mass flux condition to be added is

$$\mathbf{g} = A - 2\pi \int \mathbf{U} \cdot \mathbf{c}\, rdr = 0, \tag{A3}$$

where A is the flux at the entrance. The equation to be solved numerically is $\nabla \cdot \mathbf{J} - \mathbf{g}\nabla\mathbf{g} = 0$. The boundary conditions are

$$\partial\underline{C}/\partial r = 0 \tag{A4}$$

at the center, $r = 0$, and at the wall, $r = R$. At the entrance, the imposed condition is uniform concentration, which in the transformed variable is:

$$\underline{C}(r) = 1/c_{fd}(r), \tag{A5}$$

where the subscript fd refers to fully developed.

When the thermodynamic variable $\underline{C} = c \exp\{\Phi/D\}$ is used, events relevant to axial development are readily visualized in two dimensions. In two dimensions, diffusive and drift motions occur due to gradients of the surface, $\underline{C}(r, x)$; convection in the x direction forces the particle to experience new regions of the $\underline{C}$-surface. Surfaces of uniform $\underline{C}$ occur for two situations: when both the concentration and potential are uniform across the field, and when the concentration profile is fully developed and the potential is given by Eq. 3. These two situations represent equality of chemical potential in the lateral direction. On the average, particles starting at a given location will exhibit lateral motions that cause them to move to points on the $\underline{C}$-surface with a smaller $\underline{C}$ values. Events in a reservoir would be modeled as the first situation with uniform chemical potential: the rheological potential and concentration are uniform, so the surface is flat and lateral motions produce no redistribution. Conventional convection is respon-

sible for net particle motions (i.e., for flow into the tube). (The small differences of chemical potential due to different values of pressure and average total fluid velocity are being ignored.) Upon entering the tube, the $\underline{C}$-surface is no longer flat; the entire surface is warped, with the lowest points (depressions) corresponding to the wells of the potential function. This abrupt change is a result of assuming that the mechanical potential develops immediately and fully at the entrance plane. As can be seen by consideration of the boundary condition at the entrance, Eq. A5, the concentration immediately upon entering is uniform, but the potential is not. The $\underline{C}$-surface has depressions at the near-wall locations where the peaks of the fully developed excesses occur. During their trip through the tube, the platelets suffer lateral motions that redistribute them so as to populate the depressions. This redistribution changes the concentration, which changes $\underline{C}$ and lessens the amount of depression in the $\underline{C}$-surface. Ultimately, the $\underline{C}$-surface becomes flat in the region of fully developed flow. The key features that accompany the potential are its self-limiting nature and its compensatory action over the entire field. If some action causes the value of $\underline{C}$ to become greater than that at nearby regions, e.g., a reduction of rheological potential or an elevation of c, lateral motions will move particles away from that point and tend to flatten the $\underline{C}$-surface. In contrast to sinks or sources, which set gradients at their locations, selecting a form for a potential sets the nature of the surface over the entire field. Of course, the final amplitude also depends upon the concentration. It seems that the automatic balancing and field-wide action associated with the potential would be difficult to obtain in a model constructed with sinks and sources.

Dr. Bernard Howard provided valuable advice concerning the numerical methods, especially the inclusion of the flux balance condition that was used to stabilize the finite difference calculations.

This work was sponsored by grant HL-33100 from the National Heart, Lung, and Blood Institute.

Received for publication 12 March 1990 and in final form 5 March 1991.

REFERENCES

1. Tangelder, G. J., D. W. Slaaf, H. C. Teirlinck, R. Alewijnse, R. S. Reneman. 1982. Localization within a thin optical section of fluorescent blood platelets flowing in a microvessel. *Microvasc. Res.* 23:214–230.
2. Aarts, P. A. M. M., van den S. A. T. Broek, G. W. Prins, G. D. C. Kuiken, J. J. Sixma, and R. M. Heethaar. 1988. Blood platelets are concentrated near the wall and red blood cells, in the center in flowing blood. *Arteriosclerosis.* 8:819–824.
3. Pontius, J. 1989. Non-specific staining of platelets for use in platelet distribution studies. M. S. thesis. University of Miami, Coral Gables, FL.
4. Sparks, K. D. 1983. Platelet concentration profiles in blood flow through capillary tubes. M. S. thesis, University of Miami, Coral Gables, FL.
5. Tilles, A. W., and E. C. Eckstein. 1987. The near-wall excess of platelet-sized particles in blood flow: Its dependence on hematocrit and wall shear rate. *Microvasc. Res.* 33:211–223.
6. Eckstein, E. C., A. W. Tilles, and F. J. Millero. 1988. Conditions for the occurrence of large near-wall excesses of small particles during blood flow. *Microvasc. Res.* 36:31–39.
7. Bilsker, D. L., C. M. Waters, J. S. Kippenhan, and E. C. Eckstein. 1989. A freeze-capture method for the study of platelet-sized particle distributions. *Biorheology.* 26:1031–1040.
8. Waters, C. M., and E. C. Eckstein. 1990. Concentration profiles of platelet-sized latex beads for conditions relevant to hollow-fiber hemodialyzers. *Artif. Organs.* 14:7–13.
9. Eckstein, E.C., J. F. Koleski, and C. M. Waters. 1989. Concentration profiles of 1 and 2.5 μm beads during blood flow: hematocrit effects. *Trans. Am. Soc. Artif. Intern. Organs.* 35:188–190.
10. Palmer, A. A. 1966. Platelet and leucocyte skimming. Fourth European Conference on Microcirculation, Cambridge, England. *Bibl. Anat.* 9:300–303.
11. Blackshear, P. L., S. V. Patankar, R. W. Heil, M. Ivandvic, T. Nippoldt, and A. Rosenstein. 1978. Fluid Dynamics of Blood Cells and Applications to Hemodialysis. National Technical Information Service, Washington, DC. PB-288 587.
12. Beck, M. R., and E. C. Eckstein. 1980. Preliminary report on platelet concentration in capillary tube flows of whole blood. *Biorheology* 17:455–464.
13. Corattiyl, V., and E. C. Eckstein. 1986. Regional platelet concentration in blood flow through capillary tubes. *Microvasc. Res.* 32:261–270.
14. Turitto, V. T., A. M. Benis, and E. F. Leonard. 1972. Platelet diffusion in flowing blood. *Ind. Eng. Chem. Fundam.* 11:216–233.
15. Perkkio, J., L. J. Wurzinger, and H. Schmid-Schoenbein. 1987. Plasma and platelet skimming at T-junctions. *Thromb. Res.* 45:517–526.
16. Perkkio, J., J. Hokkanen, and R. Keskinen. 1986. Theoretical model of phase separation of erythrocytes, platelets and plasma at branches. *Med. Phys.* 13:882–886.
17. Friedman, L. I., H. Leim, E. F. Grabowski, E. F. Leonard, and C. W. McCord. 1970. Inconsequentiality of surface properties for initial platelet adhesion. *Trans. Am. Soc. Artif. Intern. Organs.* 16:63–73.
18. Goldsmith, H. L. 1971. Red cell motions and wall interactions in tube flow. *Fed. Proc.* 30:1578–1588.
19. Goldsmith, H. L., and V. T. Turitto. 1986. Rheological aspects of thrombosis and haemostasis: basic principles and applications. *Thromb. and Haemostasis.* 55:415–435.
20. Aarts, P. A. M. M., P. Steendijk, J. J. Sixma, and R. M. Heethaar. 1986. Fluid shear as a possible mechanism for platelet diffusivity in flowing blood. *J. Biomech.* 19:799–805.
21. Popel, A. S. 1989. Theory of oxygen transport to tissue. *CRC Crit. Rev. Biomed. Eng.* 17:257–321.
22. Zydney, A. L., and C. K. Colton. 1988. Augmented solute transport in the shear flow of a concentrated suspension. *PhysicoChem. Hydrodynamics.* 10:77–96.
23. Goldsmith, H. L., and S. G. Mason. 1967. The microrheology of dispersions. *In* Rheology: Theory and Applications. F. R. Eirich, editor. Academic Press, New York. 4:85–250.
24. Keller, K. H. 1971. Effect of fluid shear on mass transport in flowing blood. *Fed. Proc.* 30:1591–1599.
25. Segré, G., and A. Silberberg. 1962. Behaviour of macroscopic rigid spheres in Poiseuille flow. Parts I and II. *J. Fluid Mech.* 14:115–157.
26. Seshadri, V., and S. P. Sutera. 1968. Concentration changes of suspensions of rigid spheres flowing through tubes. *J. Colloid Interface Sci.* 27:101–110.
27. Bugliarello, G., and J. Sevilla. 1970. Velocity distribution and other characteristics of steady and pulsatile blood flow in fine glass tubes. *Biorheology.* 7:85–107.

28. Gardiner, C. W. 1985. Handbook of Stochastic Methods for Physics, Chemistry and the Natural Sciences. 2nd ed. Springer-Verlag, New York.

29. Brenner, H., and L. J. Gaydos. 1977. The constrained Brownian movement of spherical particles in cylindrical pores of comparable radius: models of the diffusive and convective transport of solute molecules in membranes and porous media. *J. Colloid Interface Sci.* 58:312–356.

30. Hetsroni, G. 1982. Handbook of Multiphase Systems. Hemisphere Publishing Corp., New York.

31. Fung, Y. C. 1984. Biodynamics. Springer-Verlag, New York.

32. Carr, R. T. 1989. Estimation of hematocrit porfile symmetry recovery length downstream from a bifurcation. *Biorheology.* 26:907–920.

33. Yum S. I. 1970. Erythrocyte-tube wall interactions in laminar flow of blood suspension. Ph. D. thesis. University of Minnesota, Minneapolis, MN.

34. Van Den Broek, C. 1982. A stochastic description of longitudinal dispersion in uniaxial flows. *Physica.* 112A:343–352.

35. Taylor, G. I. 1953. Dispersion of soluble mater in solvent flowing slowly through a tube. *Proc. R. Soc. Edinb. (Math Phys. Sci.).* 219:186–203.

36. Thacker, W. C., D. Eppel, and J. Häuser. 1986. Advective transport via error minimization: enforcing constraints of non-negativity and conservation. *Applied Math. Modelling.* 10:438–444.

37. Hochfield, E., editor. 1957. Stabilization of computer circuits. University of Chicago. United States Government Printing Office, Washington, DC. WADC Technical Report. 57-425 (AD 155740).

38. Baumgarte, J. and E. Stiefel. 1974. Examples of transformations improving the numerical accuracy of the integration of differential equations. *In* Lecture Notes in Mathematics. Vol. 364. Proceedings of the Conference on the Numerical Solution of Ordinary Differential Equations. A. Dold and B. Eckmann, editors. Springer-Verlag, New York. 207–236.

39. Rao, N. J., J. D. Borwankar, and D. Ramkrishna. 1974. Numerical solution of Ito integral equations. *SIAM (Soc. Ind. Appl. Math.) J. Control.* 12:124–139.

40. Kippenhan, J. S. 1987. Computer methods for estimating concentration profiles of platelet-sized particles in blood suspensions. M. S. thesis, University of Miami, Coral Gables, FL.

41. Silverman, B. W. 1986. Density Estimation of Statistics and Data Analysis. Chapman and Hall, New York.

42. Hubbell, J. A., and L. V. McIntire. 1986. Visualization and analysis of mural thrombogenesis on collagen, polyurethane and nylon. *Biomaterials.* 7:354–363.

43. Folie, B. J., and L. V. McIntire. 1989. Mathematical analysis of mural thrombogenesis: concentration profiles of platelet activating agents and effects of viscous shear flow. *Biophys. J.* 56:1121–1141.

44. Sakariassen, K. S., and H. R. Baumgartner. 1989. Axial dependence of platelet-collagen interactions in flowing blood: upstream thrombus growth impairs downstream platelet adhesion. *Arteriosclerosis.* 9:33–42.

45. Bagnold, R. A. 1954. Experiments on a gravity-free dispersion of large solid spheres in a Newtonian fluid under shear. *Proc. R. Soc. Edinb. (Math Phys. Sci.).* 225:49–63.

46. Seitz, F. 1948. On the theory of vacancy diffusion in alloys. *Phys. Rev.* 74:1513–1523.

47. Eckstein, E. C. 1982. Rheophoresis: a broader concept of platelet dispersivity. *Biorheology.* 19:717–724.

48. Waters, C. M. 1987. Concentration profiles of platelet-sized latex beads in blood suspensions flowing through capillary tubes. M. S. thesis. University of Miami, Coral Gables, FL.